ANALYSIS
https://doi.org/10.1038/s41893-019-0388-x
nature sustainability

Sustainable co-production of food and solar power to relax land-use constraints

Caleb K. Miskin[1,3], Yiru Li[1,3], Allison Perna[2], Ryan G. Ellis[1], Elizabeth K. Grubbs[2], Peter Bermel[2] and Rakesh Agrawal[1*]

Renewable energy could often be land constrained by the diffuse nature of renewable resources. To relax land constraints, we propose the concept of 'aglectric' farming, where agricultural land will be sustainably shared for food and energy co-production. While wind turbines on agricultural land are already put into practice, solar power production on agricultural land is still under research. Here, we propose photovoltaic systems that are suitable for installation on agricultural land. Adjusting the intensity, spectral distribution and duration of shading allows innovative photovoltaic systems to achieve significant power generation without potentially diminishing agricultural output. The feasibility of solar aglectric farms has been proven through shadow modelling. The proposed solar aglectric farms—used alone or in combination with regular solar parks or wind plants—could be a solution for a sustainable renewable economy that supports the 'full Earth' of over 10 billion people.

As the global population approaches 10 billion by the mid-century[1], supplying all the needs of the human race from the Earth's limited land area will be the essential challenge of sustainability. In a highly populated 'full Earth'[2], all available renewable energy resources will be used synergistically, while solar and wind energy will be dominant[3]. However, their power density, or rate of supplied energy per unit land area, is much more dilute than that of fossil fuels[4]. Hence, large tracts of land are required to harness solar or wind energy[5,6]. Since transmitting energy over long distances will be expensive, risky and prone to significant transmission losses, local sustainability is greatly preferred[7]. While the availability of wind energy is highly geographically limited, solar resources are accessible in most of the populated regions around the world, usually with a higher power density than wind[8,9]. Therefore, we evaluate the land feasibility of a 100% solar economy in the contiguous United States as an example, and find that it will be difficult for currently available land to meet the energy needs using current solar park designs for the entire contiguous United States and for nearly half of the individual states, which include well over half of the total US population. Barring radical improvements in agricultural output that could greatly reduce the land devoted to agriculture, the competition for land between energy and food seems inevitable, posing a major challenge to a future solar economy[10].

To address this issue, we propose the concept of the 'aglectric' farm, where agricultural land (including cropland, grassland pasture and range in this study; Supplementary Note 1) produces electricity without diminishing existing agricultural output. Both wind turbines and photovoltaic (PV) panels can be used to generate electricity on agricultural land. While wind aglectric farming is already put into practice, the use of the current PV panels is known to have a negative impact on crop growth[11–13], mainly due to shadows. Previous researchers have proposed or tested several PV and food co-production ideas, but these systems either sacrifice agricultural production or are limited to several types of shadow-tolerant crops[14–17]. For example, Fraunhofer ISE installed elevated south-facing bifacial solar panels and found yield losses of 18–19% for crops such as wheat, potatoes and celeriac growing underneath the PV array[18]. Since maintaining agricultural output (especially of major crops such as wheat, rice, soybean, and so on) is of high priority, existing PV modules and their installation practice will not enable the envisioned PV aglectric farm due to shadows. Meanwhile, wind plants require larger land area than PV parks[8,9]. Exploring the feasibility of PV aglectric farms is essential towards a post-carbon era (see Supplementary Discussion for information on wind aglectric farms). Therefore, we propose several innovative PV systems using existing and new materials, innovative installation paradigms and module designs. Through extensive modelling of PV shadows throughout a day, we show that some of our designed PV systems could mitigate the loss of solar radiation while still maintaining substantial power output. Thus, it should be possible to design and install these PV systems on agricultural land to have significant power output without potentially diminishing agricultural production. We also show that PV aglectric farms alone will have the potential of realizing a 100% solar economy without land constraint. Together with regular PV parks and wind aglectric farms, PV aglectric farms will serve as an important option for a renewable future.

Land requirements for the solar economy

PV parks in the United States generate ~4 to ~11 W m^{-2} power output when averaged over 24-h days for an entire year, with a national average of ~7 W m^{-2} (refs. [5,9]) (Supplementary Note 2). Wind plants in the United States generate ~1 W m^{-2} power output[8] (Supplementary Discussion). Since solar energy has a higher power output density and wider availability, we investigated the potential for a 100% solar-powered economy as a bookend scenario[19,20]. Although we focused on the solar end, this does not imply that wind or other renewable resources will not be used in practice. Instead, when feasible, wind and solar energy should be used to supplement each other (Supplementary Discussion).

In our projected solar economy scenario (SES), PV electricity will become the dominant form of energy supplied to end-use sectors (residential, commercial, industrial and transportation). Based on the primary energy consumption of the current fossil fuel scenario (FFS) and the energy conversion efficiencies of major steps

[1]Davidson School of Chemical Engineering, Purdue University, West Lafayette, IN, USA. [2]School of Electrical and Computer Engineering, Purdue University, West Lafayette, IN, USA. [3]These authors contributed equally: Caleb K. Miskin, Yiru Li. *e-mail: agrawalr@purdue.edu

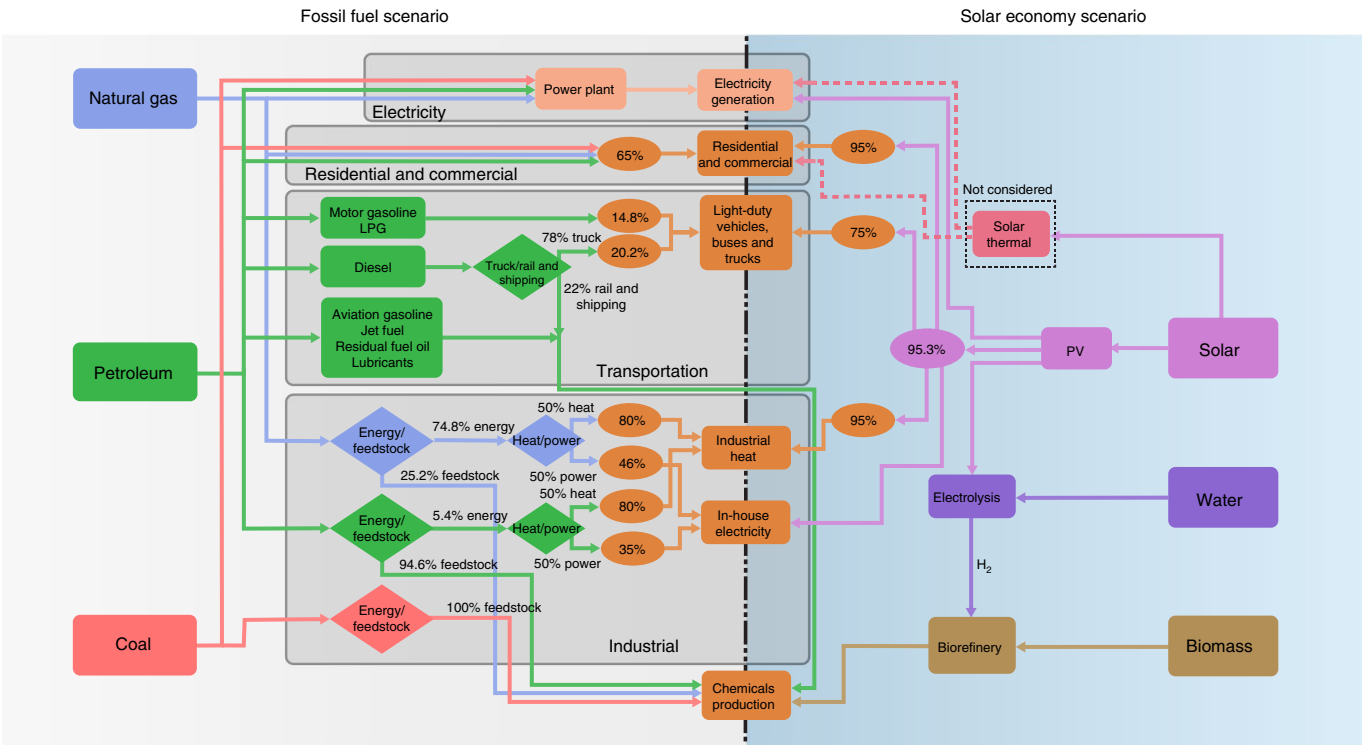

Fig. 1 | Detailed calculation model for a fossil fuel to solar energy transition. Diamonds indicate the splitting of energy use and ovals indicate efficiencies for the corresponding steps.

from primary energy to end uses in both scenarios (Fig. 1), the total power required for the contiguous United States in the SES is estimated to be 1,164 GW (Methods). Considering the intermittency and energy storage loss, an estimated total of 1,665 GW of generation is required (Supplementary Note 3)[21].

While most open land areas (forests, national and state parks, agricultural land, and so on) are not available for existing PV parks, miscellaneous land is the only available open land, which accounts for only 3.6% of the total land area of the contiguous United States[22]. Since some of the miscellaneous land, such as marshes, swamps and bare rocks, will still not be suitable for PV systems, we assume that 50% of miscellaneous land is usable for PV parks (Supplementary Note 1). Meanwhile, some urban areas could be dedicated to rooftop or building-integrated PV systems. Studies have suggested that 1–12% of urban areas could be used for PV panels[23–25].

For the entire contiguous United States, based on the total estimated SES power demand of 1,665 GW and the average power output of ~7 W m^{-2} from PV parks, besides 50% of the miscellaneous land area, ~41% of the urban area would be needed for PV parks. Even if the output of PV parks can reach 11 W m^{-2}, which is highly optimistic, the corresponding percentage of the total urban area needed is estimated to be 5.6%, in addition to 50% of the miscellaneous land. For the entire contiguous United States, this high urban land requirement reveals that the solar economy could be land constrained.

In addition, we applied the similar calculation scheme to highly populated countries such as the United Kingdom and Germany[26]. The results for the United Kingdom and Germany show that 10.2 and 12.1% of the total land will be needed for PV parks, respectively. However, 83.8% of the land in the United Kingdom and 80.7% of the land in Germany is devoted to agricultural or forest uses[27,28]; using the remaining land area for power generation is still extremely challenging.

To determine the feasibility of a local solar economy at the state level in the contiguous United States, we calculated the power density requirement for each state using the estimated solar power demand and the potentially usable land for each state. From Fig. 2a, we see that if 50% of the miscellaneous land and 5% of the urban land were available for PV systems, the power density requirement of 24 states would be greater than 11 W m^{-2}, while for nine states it would be between 7 and 11 W m^{-2}. If 15% of the urban land could be used, which is a very optimistic assumption, 20 states would still require a power density exceeding 11 W m^{-2}, while ten states would require 7–11 W m^{-2} (Fig. 2b). In either case, many of these states are relatively densely populated, such as New York, New Jersey, Maryland, Delaware, Florida and Illinois. Others, such as Indiana and Wyoming, will require high power densities, since most of their land is devoted to agriculture (cropland or pasture). For these states, additional land area besides the miscellaneous and urban land will be needed for PV installation. We also investigated cases with different percentages of miscellaneous land usage, PV power density output and energy storage efficiencies, and the results remain similar (that is, a large number of states require additional land besides miscellaneous and urban areas (Supplementary Table 3)). Since agricultural land is readily accessible, we propose to use agricultural land to build PV aglectric farms for power production while preserving food production.

PV systems for PV aglectric farms

The purpose of PV aglectric farming is engineered shadow management such that sufficient light is transmitted for equivalent crop yield while directing the remaining light for PV conversion. Shadows can be manipulated and managed through two distinct strategies: (1) current PV materials such as polysilicon, cadmium telluride and so on, plus new panel installation methods and module designs; and (2) new PV materials and module designs for optimum PV aglectric farm performance. To allow the space for crop growth, farming equipment movement on croplands and livestock activities on pastures, these PV systems will generally have to be installed at an elevated height (4 m or higher) and possibly with increased row spaces compared with ground-mounted panels in regular PV parks.

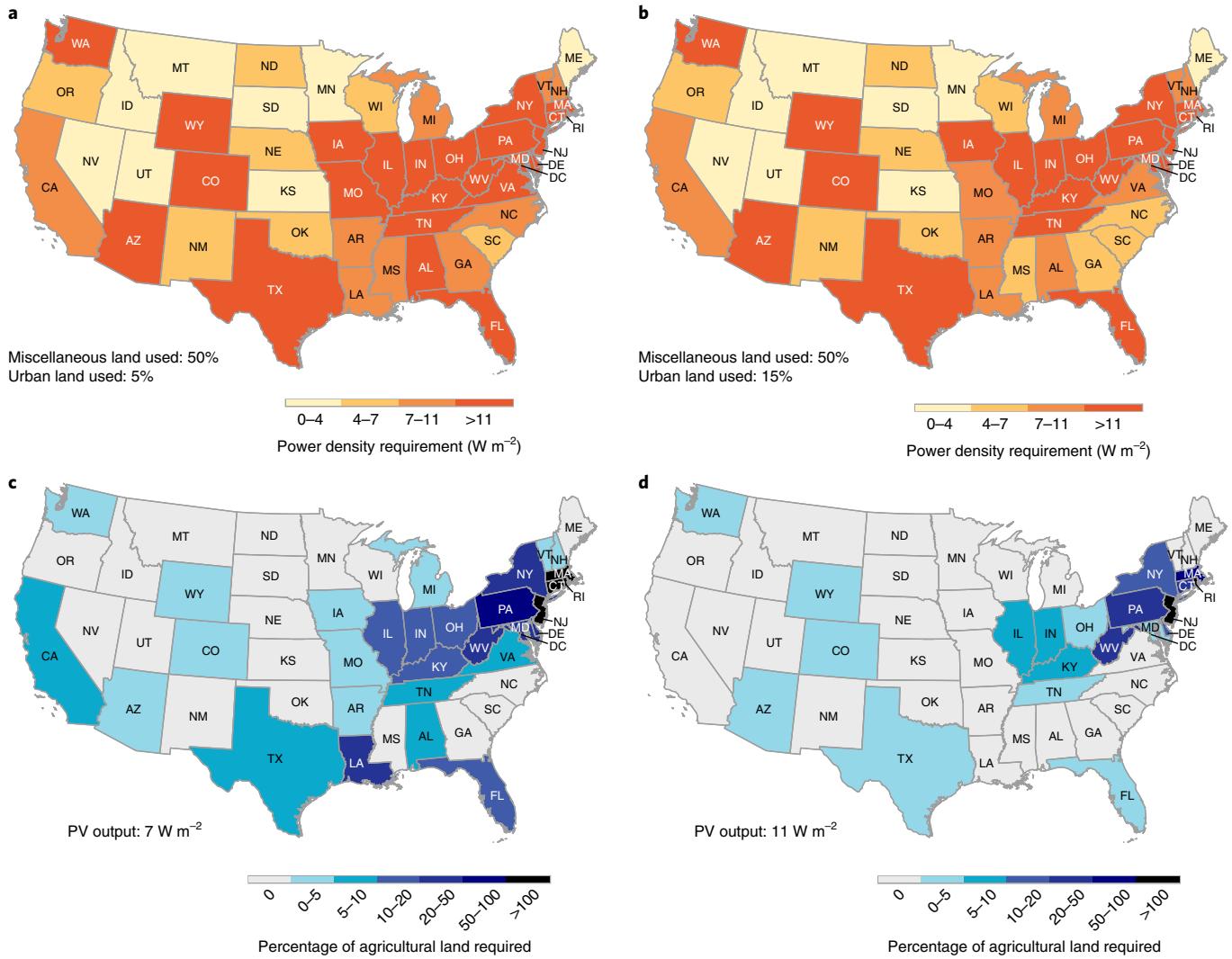

Fig. 2 | Power density requirements by state, and percentages of agricultural land required to meet states' energy needs. a,**b**, Power density requirement of each state when 50% of its miscellaneous land and 5% (**a**) and 15% of urban land (**b**) is used for PV installation. **c**,**d**, Percentages of agricultural land required in addition to 50% of miscellaneous land and 15% of urban land to meet states' local energy needs. Cases shown are for a PV power output of 7 W m^{-2} on regular PV parks (the current average PV park output) and 3.7 W m^{-2} over agricultural land (**c**), and for a PV power output of 11 W m^{-2} on regular PV parks (the upper end of current PV park output) and 5.5 W m^{-2} over agricultural land (**d**).

The installation might also help with reducing the shadow intensity on the ground.

PV systems with current PV materials and technologies. First, we considered innovative module installation and designs for commercially available materials/PV modules. In Fig. 3a, we propose a PV module design with transparent areas between solar cells for possible fixed installation. The pattern can be easily accomplished with traditional 'tiled' single-junction silicon panels. A light diffuser in the empty tiles helps distribute light beneath the panels. While various patterns could be used, a chequered pattern ensures that all crops affected by the panels' shadow receive essentially the same average illumination, and no individual plant is in intense shade for long. The percentage of filled (solar cells) versus unfilled (transparent) area could also be adjusted. In Fig. 3b, the use of a patterned PV module is applied to an east–west single-axis tracking configuration to further reduce the impact of shading. It can also be modified to become a dual-axis tracking configuration. Figure 3c utilizes vertical bifacial solar panels to capture sunlight[29]. North–south facing panels mainly capture diffuse light; however, they have the distinct advantage of allowing all direct radiation to be transmitted to the plants except for a thin line-shadow that moves throughout the day. These modules could be installed on axes that rotate slightly throughout the year, to keep the panels aligned with the Sun's path to minimize shading. A major benefit of this system is that during non-growing seasons, the panels could transition to a standard south-facing bifacial panel for increased power production during the winter months. Bifacial panels can increase power output by capturing albedo light from the rear side[30,31]. Alternatively, when the bifacial panels are installed to face east–west, as shown to the right of Fig. 3c, a peak in electricity generation is realized in the morning and evening, capturing only diffuse light at noon. When facing east–west, these panels could also be patterned as shown in Fig. 3a to further diffuse the shadow intensity.

New PV materials and module designs. Gencer et al.[10] identified several solar spectrum-splitting systems to direct photosynthetically active region (PAR) photons to food production and long-wavelength photons to solar cells for electricity generation. These structures rely on concentrating troughs that are coated with

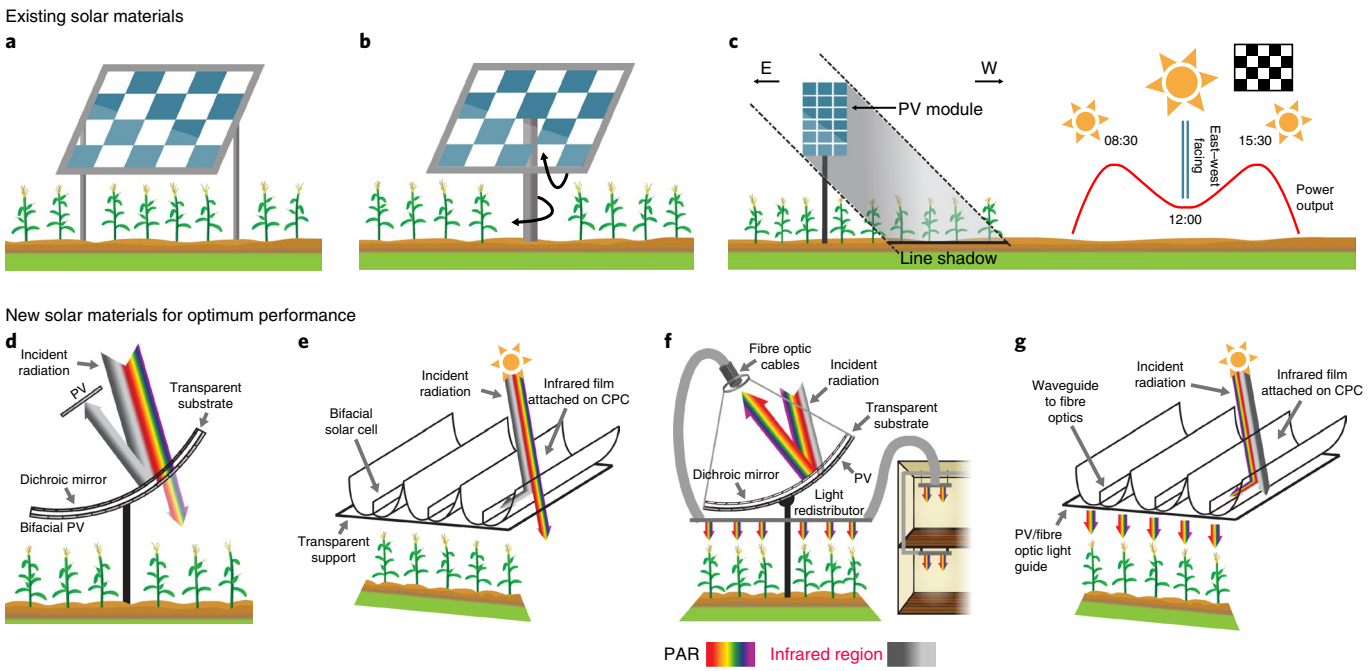

Fig. 3 | PV systems for co-production of food and energy with farmland. a–g, Fixed south-facing patterned panels (**a**), tracking patterned panels (**b**) and bificial vertical panels (**c**) can be used with existing PV materials, while short-pass tracking (**d**), short-pass non-tracking (**e**), long-pass tracking (**f**) and long-pass non-tracking (**g**) would have optimum performance with band-gap materials tailored to the incident spectrum.

well-studied dichroic materials or commercially available polymeric dichroic mirrors, to split the spectrum into the PAR and the infrared region[32–36]. In the system in Fig. 3d, a parabolic trough with a short-pass dichroic film allows the PAR to transmit to the crops below, while concentrating the infrared light on a solar cell[8]. The system in Fig. 3e uses a compound parabolic concentrator (CPC) with a short-pass dichroic film that allows the PAR through to the crops while directing a significant fraction of the incident direct infrared region to vertical bifacial cells at the centre of the CPC[32]. The CPC could have a transparent cover to keep dirt out, as well as a built-in, gravity-fed rain redistribution system. In the system shown in Fig. 3f, the PAR is reflected by a long-pass dichroic mirror attached to a fibre optic bundle, which allows for redistribution of light to the plants underneath, and potentially to vertical farms during winter months. Alternatively, during winter months when no food crops are grown, PV cells could replace the fibre optic bundles so that the light is still utilized. Figure 3g presents a system where a long-pass CPC is used to redirect the PAR to a central waveguide to redistribute light underneath, while the infrared spectrum transmits to the PV support underneath. Although they are not shown in Fig. 3, heliostats with a short-pass dichroic mirror can also be used, and the reflected long-wavelength portion could be focused on appropriate solar cells or a thermal system for concentrating solar thermal power generation. The impact of depriving plants of infrared irradiation is discussed in Supplementary Note 4.

Feasibility of PV systems based on shadow modelling

To understand the effects that solar panel array geometries have on nearby crop growth, and to check the feasibility of our selected PV systems (configurations in Fig. 3a,b), we developed a simulation that predicts the loss in incident solar energy on the underlying crops due to shading by the panels. We define the variable 'shadow depth' as the loss of incident solar energy compared with an open field; for example, if the solar irradiation at a location on a PV aglectric farm is 90% of that on an open field, the shadow depth is 10%. All configurations are elevated to 5 m to allow for navigation of agricultural equipment and to suppress the blocking of diffuse light. Both high row-spacing configurations (7.62 m) and lower row-spacing configurations (3.81 m) are simulated—the latter being representative of some existing regular PV parks[9].

Established crop growth models indicate that photosynthesis scales with the solar intensity I according to $aI/(1+bI)$, all other factors being equal. As a result, growth is linearly proportional to intensity in low-light conditions but saturates under intense light. The intensity at which crossover between these two regimes occurs varies with the crop[37]. For instance, the photosynthetic rates of cotton and rice typically saturate at approximately 650 W m^{-2} of solar irradiance, which is well below the average midday irradiance during the growing season for high-irradiance agricultural regions such as Texas and California[38,39]. Based on this model, we predict that for many commercially relevant crops, regions of high shadow depth will have low crop yield, but low levels of homogeneous shadowing may have a negligible effect on certain crop yields. This is also consistent with experience, in that annual variations of solar energy delivered over the growing season generally do not cause crop failures.

Table 1 lists the average shadow depth, its standard deviation and the percentage of land with less than 25% of shadow depth for five different PV configurations we have simulated (Methods). The standard deviation indicates the spatial homogeneity of the shadow on the ground. Figure 4 shows the spatially mapped shadow depth for selected cases in Table 1. The results in Table 1 and Fig. 4 are based on the solar radiation in the South Plains region of Texas—a region with intermediate levels of diffuse light. Simulation results for other locations with low and high levels of diffuse light are listed in Supplementary Table 1. In Table 1, cases A and C represent current fixed south-facing and east–west tracking configurations in regular PV parks with low row spacing, respectively. Cases B and E utilize the proposed design in Fig. 3a,b, respectively. An additional case D represents a continuous tracking panel with high row spacing.

The simulation result for case A shows that the average shadow depth is 35.2% and homogeneity is low (15% s.d.), and that only 41% of the land will be under <25% shadow depth (Table 1), which indicates that more than half of the land will be under intense shadow

Table 1 | Shadow depth and usable land for various PV aglectric configurations

	Configuration	Panel design	Row spacing (m)	Average shadow depth (%)	Shadow depth s.d. (%)	Land with less than 25% shadow depth (%)
A	South facing	Continuous	3.81	35.2	15.2	41.0
B	South facing	Chequered	3.81	17.6	7.6	74.7
C	East–west tracking	Continuous	3.81	31.5	0.6	0
D	East–west tracking	Continuous	7.62	21.4	0.6	100.0
E	East–west tracking	Chequered	7.62	11.5	1.1	100.0

Cases A and C represent existing PV park configurations (fixed south facing and east–west tracking, respectively). Cases B and E utilize the proposed design in Fig. 3a,b, respectively.

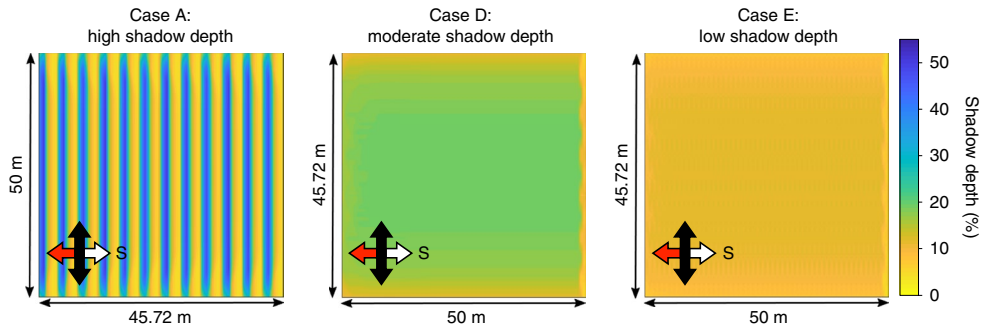

Fig. 4 | Spatially mapped shadow depth for cases A, D and E from Table 1. Case A, representing an elevated south-facing fixed latitude-tilt PV park, shows regions of high shadow depth. Case D shows the advantage of using an east–west tracking system. Case E shows the advantages gained from implementing a chequered pattern on the panels.

if a regular south-facing PV installation scheme is applied. In addition, 'trenches' of high shadow depth (>40%) exist during the entire growing season in >20% of the plot area (case A; Fig. 4). We expect that such deeply shadowed regions will experience minimal growth of many commercially relevant crops (such as soybeans). The trenches of high shadow could be one potential explanation for the observed decline in crop yield reported by Fraunhofer ISE[18]. Case C, which represents continuous tracking panels with low row spacing, shows worse results, where no land will have shadow depth lower than 25% (Table 1). Cases A and C both illustrate that regular PV parks should not be directly applied for PV aglectric farms.

In case B, which is representative of the configuration in Fig. 3a, the land area with <25% shadow depth has increased to 74.7% and the average shadow depth has reduced to 17.6%, with a reduced standard deviation of 7.6% compared with case A. This shows the effect of the reducing shadow intensity and increasing homogeneity of the chequered design. Here, we do not consider the deployment of light diffusers in the empty tiles as stated in the previous section; the chequered pattern with light diffusers will further improve the shadow distribution on the ground. From cases D and E, we can see that both continuous and chequered east–west tracking configurations with high row spacing (7.62 m) ensure that all land experiences a shadow depth <25%. The average shadow depth is low and shadow homogeneity is high in both cases. Furthermore, Fig. 4 cases D and E show that no 'trenches' of high shadow depth exist. Therefore, the potential feasibility of our newly designed systems in Fig. 3a,b is proven.

Land requirement for PV aglectric farms

We estimated the power density output from PV aglectric farms with the configurations shown in Fig. 3a–e, and results are summarized in Table 2 (Methods). Note that for the systems in Fig. 3a,b, which use currently available PV materials with a new panel design or installation method, the power output based on the active PV cell area is similar to that from the conventional PV panels, and the reduced power output based on unit land area, as shown in Table 2, is not due to the lower efficiencies of the PV cell itself. Instead, the reduction in power output density should be attributed to the 'sparse' installation (chequered design, higher row spacing, and so on).

Based on the power output numbers in Table 2, agricultural land requirement for PV aglectric farms can be calculated for the states where miscellaneous and urban land are insufficient (Supplementary Table 3). In one case, the power output from regular PV parks is assumed to be 7 W m^{-2} and the power output from PV aglectric farms is 3.7 W m^{-2}, which is the average of the lower estimated values shown in Table 2. In a more optimistic case, the power output from regular PV parks is assumed to be 11 W m^{-2} and the power output from PV aglectric farms is 5.5 W m^{-2}. For both cases, 50% of the miscellaneous land and 15% of the urban land would be used for regular PV parks, and the remaining power requirement would be fulfilled by PV aglectric farms. Figure 2c,d, respectively, shows the percentage of agricultural land required to be converted to PV aglectric farms under these two cases. We observe that the majority of states require only a small percentage of the agricultural land to satisfy their power needs. This implies that the lower power density of PV aglectric farms compared with regular PV parks is acceptable for most states, since most states have sufficiently large agricultural land areas. Furthermore, since a relatively low power output from PV aglectric farms is tolerable, row spacing between PV panels can be further enlarged to reduce the shadow intensity on the ground. However, there are states that face the challenge of land constraints in both cases, such as Massachusetts, New Jersey and Rhode Island. These states are all densely populated, highly urbanized states with a small percentage of agricultural land. For these states, PV aglectric farming alone cannot enable a 100% localized renewable economy. Importing electricity from adjacent states (or regions) and using other renewable energy such as wind could help resolve this challenge.

Table 2 | Summary of PV system characteristics and estimated PV aglectric farm power output

System (from Fig. 3)	Spectrum regions transmitted to plants in shaded region				Shade duration	Power estimate ($W m^{-2}$)	Non-growing season configuration
	Diffuse PAR	Direct PAR	Diffuse infrared region	Direct infrared region			
a	Yes	Yes	Yes	Yes	Constant	3.5–5.5	None
b	Yes	Yes	Yes	Yes	Mobile	2.3–3.5	None
c (north–south facing)	Yes	Yes	Yes	Yes	Negligible shade	4.9–6.7	Traditional bifacial
c (east–west facing)	Yes	Yes	Yes	Yes	Mobile	4.1–6.0	
d	Yes	Yes	No	No	Mobile	3.6–5.7	None
e	Yes	Yes	No	No	Constant	3.6–5.7	None
f	No	Yes	No	No	Mobile	–	Concentrating PV system
g	No	Yes	No	No	Constant	–	Concentrating PVsystem

While we focus on a bookend case for the contiguous United States, our methods and results also show how PV aglectric farms could be useful across most countries and regions experiencing land constraints in sustainable food and energy production. Furthermore, the concept of aglectric farming can also be applied to multiple renewable energy resources, such as wind energy. Given that PV aglectric farming alone has the potential of enabling a 100% solar economy for most states in the contiguous United States, synergistic power production from multiple renewable energy resources on agricultural land will have a huge impact in realizing a future renewable energy roadmap.

Exploring synergy between wind and PV aglectric farms

Since wind aglectric farms are already being used in certain parts of the United States, it is worthwhile to explore the synergy between PV and wind aglectric farms (Supplementary Discussion). The actual power output density from wind aglectric farms of ~1 $W m^{-2}$ is lower than our estimated power density of 2.3–6.7 $W m^{-2}$ from the PV aglectric farms. Also, the availability of wind resource is geographically restricted. We can make the following two observations.

First, considering the case in the previous section where the power density from PV aglectric farms is 3.7 $W m^{-2}$, for the states where PV aglectric farms require less than ~27% of agricultural land, wind aglectric farms with a power density of 1 $W m^{-2}$ can also meet the power demand. In such a scenario, wind aglectric farms could cover up to 100% of the available agricultural land area and could be used interchangeably with PV aglectric farms. For regions that are relatively rich in wind resource, there is a choice between wind and PV aglectric farms to solve the land constraint. Examples include the states of Wyoming, Colorado and Texas, where wind and solar could be used in any proportion. However, for states where wind resources are limited, even when PV aglectric farms require less than ~27% of the agricultural land area, it will be essential to deploy PV panels on agricultural land. Such examples include Kentucky, Tennessee, Alabama, Florida and Virginia.

Second, for states where >27% of the agricultural land area is need for PV aglectric farms, wind aglectric farms alone will be unable to meet the entire demand of energy. A synergy between the two aglectric farms that cannot be ignored stems from the fact that wind energy can also be available during periods when solar energy is not. Furthermore, it may be possible to install both wind turbines and PV panels simultaneously on an aglectric farm. This will impact not only the power output from an aglectric farm but its availability pattern during an average 24-h day. The availability pattern will influence energy storage and associated implications. Further study should account for these factors.

Aglectric farm vision

In this work, we show that PV aglectric farming is a viable solution to relax the land constraint for a renewable future. PV aglectric farms, wind aglectric farms and regular PV parks will be used according to the local renewable resource and land availability. Besides removing the land constraint, additional benefits of aglectric farms (PV, wind, and even other renewables) are anticipated. For most non-tropical countries, agricultural land is used only for the growing season, but aglectric farms will allow agricultural land to be productive all year (by adding electricity production beyond the growing season), potentially stimulating the economy of rural farming communities by possibly increasing incomes for aglectric farm adopters.

Aglectric farming could also enable a new food, energy and water nexus in which the electricity generated on farms is utilized locally for water management, fertilizer production/recovery and bio-based chemical production. The envisioned aglectric farms will enable a 'micro-grid' system interacting with a much larger-scale economic system, including the adjoining urban centres, and finally at the state and national levels. This will enable a renewable economy for a future 'full Earth' scenario.

Methods

Land requirement analysis. To examine the land requirement for a solar economy, the power requirement needs to be estimated first. Two scenarios—the current FFS and the projected SES—are considered in our power requirement estimation. Energy consumption data of 2014 from the Energy Information Administration (EIA)[40] were adopted for the FFS, and the energy demand for SES was estimated based on these data. In the SES, only PV panels were deployed for solar energy conversion for the purpose of this study. Concentrating solar thermal power facilities and small-scale solar thermal heating (for example, for residential heating) were not used in our analysis. For the transition from the FFS to the SES, fossil fuels were completely replaced by photovoltaics, while other energy resources used in the FFS, such as wind and hydro power, were assumed to remain at the same utilization in the SES. To maintain the current lifestyle and life quality, the end-use demands were kept the same for the FFS and the SES.

The transition to a solar economy will reshape the current energy supply and consumption infrastructure. In the FFS, fossil fuels as energy resources are either used for power generation or directly supplied to end-use sectors. Now that we have assumed photovoltaics as the only method for solar harnessing and conversion, electricity will become the form of energy ultimately supplied to end uses, and nearly all of the end-use facilities will be electrified in the SES[19]. Systems that might not be feasibly electrified, such as air transportation, are taken to be powered by synthetic fuels synthesized from biomass[41,42]. In addition, a small proportion of fossil resources are consumed as chemical feedstocks in the FFS, and these fossil resources are replaced with biomass in the SES. To look at the future solar electricity demand, a detailed examination of each end-use sector was performed. In our model, we treated power generation as a separate sector, and only direct primary energy consumption was considered for the residential, commercial, industrial and transportation sectors. Chemical and fuel production from biomass was also treated as a standalone sector. Electricity demand in the SES to replace fossil fuels in the FFS was examined for each sector, and the total

electricity demand was the sum of electricity demand in each sector calculated using the following equation:

$$E^{\mathrm{SES}} = \sum_k E_k^{\mathrm{SES}}$$

where k represents electricity, residential, commercial, transportation, industrial, chemical and fuel demands, and where E^{SES} represents the total electricity demand from photovoltaics in the SES. E_k^{SES} represents the electricity demand for sector k in the SES.

For the electricity sector (k = electricity), power generation data in the FFS are from the EIA[43]. We assume the electricity flow to be the same after generation, whether this is from a fossil fuel-powered plant (FFS) or PV parks (SES), including the same transmission and distribution loss and the same end-use electricity conversion efficiency. As a result, the electric power generated from fossil fuels can be simply replaced with the same amount of electricity generated from photovoltaics. Therefore, the total electricity from photovoltaics needed to replace the electricity from fossil fuels in the FFS is calculated using the following equation:

$$E_{\mathrm{electricity}}^{\mathrm{SES}} = E_{\mathrm{electricity}}^{\mathrm{FFS}}$$

where $E_{\mathrm{electricity}}^{\mathrm{FFS}}$ represents the electricity generated from fossil fuels in the year 2014.

For the residential (k = residential) and commercial (k = commercial) sector, the SES electricity requirement is estimated by ensuring that the end-use energy consumptions are the same for the FFS and SES under different energy conversion efficiencies. The estimation paradigm is expressed by the following equation:

$$E_k^{\mathrm{SES}}\eta_k^{\mathrm{SES}}\eta_{\mathrm{transmission}}^{\mathrm{SES}} = \sum_i E_{i,k}^{\mathrm{FFS}}\eta_{i,k}^{\mathrm{FFS}}$$

where the subscript i refers to the fossil fuel (i = coal, petroleum or natural gas). $E_{i,k}^{\mathrm{FFS}}$ refers to the energy consumption by fossil fuel i in the FFS in sector k, $\eta_{i,k}^{\mathrm{FFS}}$ refers to the energy conversion efficiency from fossil fuel i to the end use in the FFS in sector k, η_k^{SES} refers to the energy conversion efficiency from electricity to the end use in the SES in sector k and $\eta_{\mathrm{transmission}}^{\mathrm{SES}}$ refers to the transmission and distribution efficiency for the electrical grid in the SES. Fossil fuels supplied directly to residential and commercial sectors are generally used as heat. The end-use efficiency for fossil fuels is estimated as 65% for these sectors in FFS ($\eta_{i,\mathrm{residential}}^{\mathrm{FFS}} = \eta_{i,\mathrm{commercial}}^{\mathrm{FFS}} = 65\%$)[44]. After switching to SES, electrical heating is much more efficient and a 95% efficiency is assumed ($\eta_{\mathrm{residential}}^{\mathrm{SES}} = \eta_{\mathrm{commercial}}^{\mathrm{SES}} = 95\%$). The transmission and distribution loss of electrical grid is taken to be 4.7%[45]; therefore, the value of $\eta_{\mathrm{transmission}}^{\mathrm{SES}}$ is 95.3%.

For the transportation sector, only natural gas and petroleum are consumed according to the EIA's energy consumption data. Moreover, as most natural gas consumption is attributed to the operation of pipelines, primarily in compressors, natural gas consumption in the transportation sector is negligible in the SES[40]. Therefore, only petroleum is considered here in the transportation sector. The estimation of electricity demand for the transportation sector is also achieved by equating end-use consumption for the FFS and SES. However, in the transportation sector, only part of the petroleum consumption can be directly replaced by electricity from photovoltaics. The electricity demand is calculated by the following equations:

$$E_{j,\mathrm{transportation}}^{\mathrm{SES}}\eta_{\mathrm{transportation}}^{\mathrm{SES}}\eta_{\mathrm{transmission}}^{\mathrm{SES}} = E_{j,\mathrm{transportation}}^{\mathrm{FFS}}f_j\eta_{j,\mathrm{transportation}}^{\mathrm{FFS}}$$

$$E_{\mathrm{transportation}}^{\mathrm{SES}} = \sum_j E_{j,\mathrm{transportation}}^{\mathrm{SES}}$$

where the subscript j refers to a specific category of petroleum (motor gasoline, liquefied petroleum gas (LPG) or diesel). For the transportation sector, only light-duty vehicles, buses and trucks are projected to be replaced by electrical vehicles, and these means of transportation are powered by motor gasoline, LPG and diesel in the FFS. Other means of transportation, such as air and marine vessels, will not be easily electrified, and the fuels for them are to be produced from biomass, which will be discussed in the chemical and fuel production sector. In the equations above, $E_{j,\mathrm{transportation}}^{\mathrm{SES}}$ is the electricity demand to replace fuel j in the SES for the transportation sector, $\eta_{\mathrm{transportation}}^{\mathrm{SES}}$ is the efficiency of electrical vehicles, $E_{j,\mathrm{transportation}}^{\mathrm{FFS}}$ is the energy consumption by fuel j in the FFS for the transportation sector, f_j is the fraction of fuel j that is consumed by means of transportation that could be electrified (for example, 78% of the diesel is consumed by trucks[46], which can be replaced with electrical vehicles, and the rest of diesel consumption by ships will not be replaced by electricity; therefore, $f_{\mathrm{diesel}} = 78\%$) and $\eta_{j,\mathrm{transportation}}^{\mathrm{FFS}}$ is the efficiency of an internal combustion engine powered by fuel j. In our estimation: all of the motor gasoline and LPG for transportation can be replaced by electricity, and diesel consumed by trucks can also be replaced ($f_{\mathrm{motor\ gasoline}} = f_{\mathrm{LPG}} = 100\%$; $f_{\mathrm{diesel}} = 78\%$[46]); the grid-to-wheel efficiency of electrical vehicles is assumed to be 75% ($\eta_{\mathrm{transportation}}^{\mathrm{SES}} = 75\%$)[47]; and internal combustion engine efficiencies average 14.8% for gasoline (LPG) engines and 20.2% for diesel engines, respectively (that is, $\eta_{\mathrm{motor\ gasoline,transportation}}^{\mathrm{FFS}} = \eta_{\mathrm{LPG,transportation}}^{\mathrm{FFS}} = 14.8\%$; and $\eta_{\mathrm{diesel,transportation}}^{\mathrm{FFS}} = 20.2\%$)[48].

For the industrial sector, fossil fuels are used as either energy sources or feedstock in the FFS. Fossil fuels used as energy resources are to be replaced by electricity, while those used as chemical feedstocks will be discussed later in the chemical and fuel production sector. The ratio of energy to feedstock in each state is assumed to be identical to the national ratio in our calculation. For the fossil fuels supplied as energy, they can be consumed for both heat and in-house generated power. The electricity demand in the SES for the industrial sector is estimated using the following equations:

$$E_{\mathrm{heat,\ industrial}}^{\mathrm{SES}}\eta_{\mathrm{heat,\ industrial}}^{\mathrm{SES}}\eta_{\mathrm{transmission}}^{\mathrm{SES}} = \sum_i E_{i,\mathrm{industrial}}^{\mathrm{FFS}}g_{i,\mathrm{energy}}h_{i,\mathrm{heat}}\eta_{i,\mathrm{heat,\ industrial}}^{\mathrm{FFS}}$$

$$E_{\mathrm{power,\ industrial}}^{\mathrm{SES}}\eta_{\mathrm{transmission}}^{\mathrm{SES}} = \sum_i E_{i,\mathrm{industrial}}^{\mathrm{FFS}}g_{i,\mathrm{energy}}h_{i,\mathrm{power}}\eta_{i,\mathrm{power,\ industrial}}^{\mathrm{FFS}}$$

$$E_{\mathrm{industrial}}^{\mathrm{SES}} = E_{\mathrm{heat,\ industrial}}^{\mathrm{SES}} + E_{\mathrm{power,\ industrial}}^{\mathrm{SES}}$$

where the subscript i refers to the fossil fuel (i = coal, petroleum or natural gas). $E_{\mathrm{heat,\ industrial}}^{\mathrm{SES}}$ and $E_{\mathrm{power,\ industrial}}^{\mathrm{SES}}$ refer to the electricity requirement in the SES to replace fossil fuels for industrial heat and in-house power generation, respectively. $\eta_{\mathrm{heat,\ industrial}}^{\mathrm{SES}}$ is the electrical heating efficiency in the industrial sector in the SES, which is assumed to be 95%. $E_{i,\mathrm{industrial}}^{\mathrm{FFS}}$ is the energy consumption of fuel i for the industrial sector in the FFS; $g_{i,\mathrm{energy}}$ is the fraction of fuel i consumed as energy (in our study, $g_{\mathrm{natural\ gas,energy}} = 74.8\%$, $g_{\mathrm{petroleum,energy}} = 5.4\%$ and $g_{\mathrm{coal,energy}} = 0$ for every state[46]). $h_{i,\mathrm{heat}}$ and $h_{i,\mathrm{power}}$ are the fractions of fuel i consumed by industrial heat and in-house power generation, respectively. We assume $h_{i,\mathrm{heat}} = h_{i,\mathrm{power}} = 50\%$. $\eta_{i,\mathrm{heat,\ industrial}}^{\mathrm{FFS}}$ and $\eta_{i,\mathrm{power,\ industrial}}^{\mathrm{FFS}}$ are the energy conversion efficiencies of fuel i to industrial heat and power, respectively ($\eta_{i,\mathrm{heat,\ industrial}}^{\mathrm{FFS}} = 80\%$, $\eta_{\mathrm{natural\ gas,power,\ industrial}}^{\mathrm{FFS}} = 46\%$ and $\eta_{\mathrm{petroleum,power,\ industrial}}^{\mathrm{FFS}} = 35\%$[40]).

For chemical and fuel production, chemical feedstocks from fossil fuels and fuels for transportation that cannot easily by electrified is produced from biomass in the SES[49]. The biomass required for the chemical and fuel production in the SES is estimated to be ~857 million tonnes. According to the US Department of Energy, the sustainably available biomass production will have the potential of over 1 billion tonnes by 2040[50,51]. Therefore, there will be sufficient biomass for chemical and fuel production for the SES. Since biomass is easy to transport, we do not consider the local availability of biomass here. Also, as sustainably available biomass is used, its production will not compete with normal food and forestry production. Furthermore, as our goal of aglectric farming is to not negatively impact the growth of plants, we do not consider the competition for land between biomass production and power generation.

Since these chemicals and fuels in the FFS are mainly hydrocarbons, we assume that these fossil fuels are purely composed of CH_2 units. Typical biomass is composed of CH_2O units; thus, the oxygen needs to be removed by biorefining. In biorefining, H_2 is obtained from water electrolysis and used to remove oxygen in biomass[21]. We can estimate the energy requirement of biorefining to replace fossil fuel feedstocks by determining the amount of H_2 required according to the amount of biomass to be upgraded, then calculating the electricity needed for water electrolysis. This estimation can be expressed by the following equation:

$$E_{\mathrm{chemical\ and\ fuel}}^{\mathrm{SES}} = \frac{W_{\mathrm{chemical\ and\ fuel}}^{\mathrm{FFS}}}{M_{\mathrm{CH_2}}} \times \Delta H_{\mathrm{water\ electrolysis}}$$

where $W_{\mathrm{chemical\ and\ fuel}}^{\mathrm{FFS}}$ is the total mass of fossil fuels used as chemical and fuels in the FFS, $M_{\mathrm{CH_2}}$ is the molar mass of the CH_2 unit, and $\Delta H_{\mathrm{water\ electrolysis}}$ is the energy demand for producing 1 mol of hydrogen by water electrolysis.

By examining each sector, we can estimate the total electricity demand for the SES and, since our land requirement estimation is based on the power output of PV parks, we would like to know the power demand for the SES. The total power demand for the SES can be obtained by averaging the total electricity demand over the entire year:

$$P^{\mathrm{SES}} = \frac{E^{\mathrm{SES}}}{T}$$

where P^{SES} is the total power demand in the SES and T is the total time of a year. The calculation of power demand considering storage efficiency is elaborated in Supplementary Note 3. The range of storage efficiencies we use is based on current storage methods.

Shadow simulation. The shadow depth was calculated for simple panel configurations and is displayed in a top-down view for 50 m × 45.72 m farm plots to show edge effects (Fig. 4). To eliminate the effect of plot size on shadow depth averages and standard deviation, calculations were performed using infinite periodicity (Table 1). For the chequered pattern, we employed with transparent spacers, each with dimensions of 0.25 m × 0.25 m (Table 1). The Haurwitz clear sky irradiance model and the Orgill and Hollands model for determining diffuse horizontal irradiance have been implemented for three agriculturally productive locations in Indiana (40.4° N, 86.9° W), Texas (33.5° N, 101.8° W) and California

(36.6° N, 119.9° W) via PVLIB—a Sandia-originated MATLAB open-source library for photovoltaics modelling[52]. Considering the high elevation of the panels necessary for navigation by farm equipment, it is assumed that diffuse light is uniformly distributed on the ground. The amount of diffuse light was determined by subtracting the diffuse fraction incident on PV panels, as calculated by the Perez model, from the total diffuse light for each time step. Tracking PV systems were modelled with the same dimensionality as the south-facing fixed systems (1.5-m-wide modules, infinitely long), and with a ±90° range of motion. Shadow position was calculated using the ray-tracing methodology, which models the Sun as a plane source with a variable position depending on the time of day, generated from PVLIB for the locations listed above on 1 June 2018. The ground was divided into finite spatial elements of identical size for incident energy integration, which was calculated with a time resolution of 1 min. The shadow depth was defined as the percentage reduction in incident energy at a given location over 1 d compared with the open field case. The averaged shadow depth in Table 1 refers to the average shadow depth of all spatial finite elements, calculated as a summation of the shadow depth values for all elements and divided by the number of elements. The shadow depth standard deviation in Table 1 is the standard deviation of the values of shadow depth across all spatial finite elements. This translates to the spatial homogeneity of the shadow.

Power output of PV aglectric farms. First, we estimated the power density output from PV aglectric farms (Table 1), and from there we obtained the power output estimation for the systems in Fig. 3a,b. For all of the cases in Table 1, the power output was calculated together with the shadow simulation. The simulation methods and parameters are explained above. The simulation results are listed in Supplementary Table 2. In Supplementary Table 2, the power output numbers in the column 'Simulated power output' are based on the solar irradiation data for the South Plains region of Texas on 1 June 2018, which are not the required yearly averages. However, we assume that the simulated power output ratio between various cases in Table 1 remains valid after averaging. From the cases for other locations (Indiana and California) shown in Supplementary Table 1, we can see that the simulated power output ratio between various cases in Table 1 remain valid for different locations. This is reasonable because the different power output for different cases at one location is only caused by the spatial arrangement of panels. A correction was made for these simulated results, and the correct power output numbers are listed in the column 'Corrected power output'. Case A is the most representative case of regular PV parks, and has a power output of 7–11 W m^{-2}. Therefore, the simulated power output of 11.8 W m^{-2} should be corrected to 7–11 W m^{-2} (where 7 and 11 W m^{-2} are the lower and upper estimates, respectively). The simulated power output in case B through case E can be corrected by the same lower and upper estimate factors: 0.59 (7/11.8) and 0.93 (11/11.8), respectively.

Since cases B and E in Table 1 (and Supplementary Table 1) represent the PV configurations in Fig. 3a,b, we obtain estimations of power output for Fig. 3a,b of 3.5–5.5 and 2.3–3.5 W m^{-2}, respectively.

For the PV system shown in Fig. 3c that uses vertical bifacial panels facing east–west, the output is estimated using the model of Sun et al. and the Purdue University Bifacial Module Calculator[29,30]. Using this model for several representative meteorological conditions yields estimates in the range of 4.1–6.0 W m^{-2}. The north–south-facing, non-chequered vertical bifacial configuration of Fig. 3c uses the diffusive part of the solar insolation only. We assume the panels are orientated at all times such that they receive no direct insolation. In this scenario, we can use the model of Khan et al.[31] to estimate the power output, except that direct insolation is only absorbed indirectly via albedo light. Depending on meteorological conditions, we estimate a power output of 4.9–6.7 W m^{-2}. Further details on the power modelling for bifacial PV systems can be found in the Supplementary Methods.

Now, we consider the PV systems from Fig. 3d,e that require new PV materials for optimum performance. For example, Gencer et al.[10] calculated maximum recoverable power from a single-junction solar cell to be 161 W m^{-2} (note that this number is based on cell area instead of land area) for a direct solar insolation of 1,000 W m^{-2} in the short-pass tracking configuration shown in Fig. 3d, with the PAR portion terminating at a wavelength of 750 nm and a concentration factor of 20. The corresponding maximum recoverable power from a conventional single-junction solar cell with the entire incident solar spectrum is ~310 W m^{-2}. If we assume a PV installation of Fig. 3d on a PV aglectric farm with an actual to maximum theoretical power output ratio of 0.52 (160/310), we would expect a power output of ~3.6–5.7 W m^{-2} (based on 7–11 W m^{-2}). The power output estimation for the PV system in Fig. 3e follows the same method.

Data availability

The data used in this analysis were obtained from the references as noted. Any additional data needed to reproduce or support this work can be obtained from the corresponding author on reasonable request.

Code availability

The code required to reproduce this work is available from the corresponding author on reasonable request.

Received: 25 October 2018; Accepted: 27 August 2019;
Published online: 7 October 2019

References

1. UN Department of Economic and Social Affairs *World Population Prospects: The 2017 Revision—Key Findings and Advance Tables* Working Paper No. ESA/P/WP/248 (2017).
2. Tilman, D. Food & health of a full Earth. *Daedalus* **144**, 5–7 (2015).
3. Jacobson, M. Z. et al. 100% clean and renewable wind, water, and sunlight all-sector energy roadmaps for 139 countries of the world. *Joule* **1**, 108–121 (2017).
4. Smil, V. *Power Density: A Key to Understanding Energy Sources and Uses* (MIT Press, 2015).
5. MacKay, D. J. C. Solar energy in the context of energy use, energy transportation and energy storage. *Phil. Trans. R. Soc. A* **371**, 20110431 (2013).
6. Capellán-Pérez, I., de Castro, C. & Arto, I. Assessing vulnerabilities and limits in the transition to renewable energies: land requirements under 100% solar energy scenarios. *Renew. Sust. Energy Rev.* **77**, 760–782 (2017).
7. Macilwain, C. Energy: supergrid. *Nature* **468**, 624–625 (2010).
8. Denholm, P., Hand, M., Jackson, M. & Ong, S. *Land use Requirements of Modern Wind Power Plants in the United States* Technical Report NREL/TP-6A2-45834 (National Renewable Energy Laboratory, 2009).
9. Ong, S., Campbell, C., Denholm, P., Margolis, R. & Heath, G. *Land-Use Requirements for Solar Power Plants in the United States* Technical Report NREL/TP-6A20-56290 (National Renewable Energy Laboratory, 2013).
10. Gençer, E. et al. Directing solar photons to sustainably meet food, energy, and water needs. *Sci. Rep.* **7**, 3133 (2017).
11. Armstrong, A., Nicholas, J. O. & Jeanette, W. Solar park microclimate and vegetation management effects on grassland carbon cycling. *Environ. Res. Lett.* **11**, 074016 (2016).
12. Marrou, H., Guilioni, L., Dufour, L., Dupraz, C. & Wéry, J. Microclimate under agrivoltaic systems: is crop growth rate affected in the partial shade of solar panels? *Agric. Meteorol.* **177**, 117–132 (2013).
13. Marrou, H., Dufour, L. & Wéry, J. How does a shelter of solar panels influence water flows in a soil–crop system? *Eur. J. Agron.* **50**, 38–51 (2013).
14. Goetzberger, A. & Zastrow, A. On the coexistence of solar-energy conversion and plant cultivation. *Int. J. Sol. Energy* **1**, 55–69 (1982).
15. Dupraz, C. et al. Combining solar photovoltaic panels and food crops for optimising land use: towards new agrivoltaic schemes. *Renew. Energy* **36**, 2725–2732 (2011).
16. Dinesh, H. & Pearce, J. M. The potential of agrivoltaic systems. *Renew. Sust. Energy Rev.* **54**, 299–308 (2016).
17. Valle, B. et al. Increasing the total productivity of a land by combining mobile photovoltaic panels and food crops. *Appl. Energy* **206**, 1495–1507 (2017).
18. Fraunhofer Institute for Solar Energy Systems. Harvesting the Sun for power and produce—agrophotovoltaics increases the land use efficiency by over 60 percent. *Fraunhofer ISE* https://www.ise.fraunhofer.de/en/press-media/press-releases/2017/harvesting-the-sun-for-power-and-produce-agrophotovoltaics-increases-the-land-use-efficiency-by-over-60-percent.html (2017).
19. Agrawal, R. & Singh, N. R. Solar energy to biofuels. *Annu. Rev. Chem. Biomol. Eng.* **1**, 343–364 (2010).
20. Agrawal, R. & Mallapragada, D. S. Chemical engineering in a solar energy-driven sustainable future. *AIChE J.* **56**, 2762–2768 (2010).
21. Al-Musleh, E. I., Mallapragada, D. S. & Agrawal, R. Continuous power supply from a baseload renewable power plant. *Appl. Energy* **122**, 83–93 (2014).
22. Nickerson, C., Ebel, R., Borchers, A. & Carriazo, F. *Major Uses of Land in the United States, 2007* (USDA Economic Research Service, 2011).
23. Ordóñez, J. et al. Analysis of the photovoltaic solar energy capacity of residential rooftops in Andalusia (Spain). *Renew. Sust. Energy Rev.* **14**, 2122–2130 (2010).
24. Hong, T., Lee, M., Koo, C., Kim, J. & Jeong, K. Estimation of the available rooftop area for installing the rooftop solar photovoltaic (PV) system by analyzing the building shadow using hillshade analysis. *Energy Procedia* **88**, 408–413 (2016).
25. Izquierdo, S., Montañés, C., Dopazo, C. & Fueyo, N. Roof-top solar energy potential under performance-based building energy codes: the case of Spain. *Sol. Energy* **85**, 208–213 (2011).
26. *World Energy Balances 2017: Overview* (International Energy Agency, 2017).
27. The World Bank *Agricultural Land (% of Land Area)* (Food and Agriculture Organization, 2018); https://data.worldbank.org/indicator/AG.LND.AGRI.ZS?view=chart
28. The World Bank *Forest Area (% of Land Area)* (Food and Agriculture Organization, 2018); https://data.worldbank.org/indicator/AG.LND.FRST.ZS?view=chart

29. Sun, X., Khan, M. R., Deline, C. & Alam, M. A. Optimization and performance of bifacial solar modules: a global perspective. *Appl. Energy* **212**, 1601–1610 (2018).
30. Zhao, B., Sun, X., Khan, M. R. & Alam, M. A. Purdue University bifacial module calculator (PUB). *nanoHUB* https://nanohub.org/resources/pub (2018).
31. Khan, M. R., Hanna, A., Sun, X. & Alam, M. A. Vertical bifacial solar farms: physics, design, and global optimization. *Appl. Energy* **206**, 240–248 (2018).
32. Ulavi, T. U., Davidson, J. H. & Hebrink, T. Analysis of a hybrid PV/T concept based on wavelength selective films. *J. Sol. Energy Eng.* **136**, 031009 (2014).
33. Charalambous, P. G., Maidment, G. G., Kalogirou, S. A. & Yiakoumetti, K. Photovoltaic thermal (PV/T) collectors: a review. *Appl. Therm. Eng.* **27**, 275–286 (2007).
34. Ilic, O. et al. Tailoring high-temperature radiation and the resurrection of the incandescent source. *Nat. Nanotechnol.* **11**, 320–324 (2016).
35. Imenes, A. G. & Mills, D. R. Spectral beam splitting technology for increased conversion efficiency in solar concentrating systems: a review. *Sol. Energy Mater. Sol. Cells* **84**, 19–69 (2004).
36. Yu, Z. J., Fisher, K. C., Wheelwright, B. M., Angel, R. P. & Holman, Z. C. PV mirror: a new concept for tandem solar cells and hybrid solar converters. *IEEE J. Photovolt.* **5**, 1791–1799 (2015).
37. McCree, K. J. The action spectrum, absorptance and quantum yield of photosynthesis in crop plants. *Agric. Meteorol.* **9**, 191–216 (1971).
38. *POWER Project Data Sets* (NASA Langley Research Center, 2018); https://power.larc.nasa.gov/
39. Jose, B. S. Agroforestry for ecosystem services and environmental benefits: an overview. *Agrofor. Syst.* **76**, 1–10 (2004).
40. *State Energy Data System (SEDS): 1960–2014 (Complete)* (US Energy Information Administration, 2017); https://www.eia.gov/state/seds/seds-data-complete.php?sid=US#Consumption
41. Agrawal, R. & Singh, N. R. Synergistic routes to liquid fuel for a petroleum-deprived future. *AIChE J.* **55**, 1898–1905 (2009).
42. Agrawal, R., Singh, N. R., Ribeiro, F. H. & Delgass, W. N. Sustainable fuel for the transportation sector. *Proc. Natl Acad. Sci. USA* **104**, 4828–4833 (2007).
43. *Net Generation by State by Type of Producer by Energy Source* (US Energy Information Administration, 2016); https://www.eia.gov/electricity/data/state/
44. *Energy Flow Charts* (Lawrence Livermore National Laboratory, 2016); https://flowcharts.llnl.gov/commodities/energy
45. *How Much Electricity is Lost in Transmission and Distribution in the United States?* (US Energy Information Administration, 2017); https://www.eia.gov/tools/faqs/faq.php?id=105&t=3
46. *Annual Energy Outlook 2016* (US Energy Information Administration, 2017).
47. Poullikkas, A. Sustainable options for electric vehicle technologies. *Renew. Sust. Energy Rev.* **41**, 1277–1287 (2015).
48. An, F. & Santini, D. *Assessing Tank-to-Wheel Efficiencies of Advanced Technology Vehicles* Technical Paper 2003-01-0412 (SAE International, 2003).
49. Singh, N. R., Delgass, W. N., Ribeiro, F. H. & Agrawal, R. Estimation of liquid fuel yields from biomass. *Environ. Sci. Technol.* **44**, 5298–5305 (2010).
50. Efroymson, R. A. et al. *2016 Billion-Ton Report: Advancing Domestic Resources for a Thriving Bioeconomy, Volume 2: Environmental Sustainability Effects of Select Scenarios from Volume 1* No. ORNL/TM-2016/727 (Oak Ridge National Laboratory, Argonne National Laboratory, National Renewable Energy Laboratory & Pacific Northwest National Laboratory, 2017).
51. Parsell, T. et al. A synergistic biorefinery based on catalytic conversion of lignin prior to cellulose starting from lignocellulosic biomass. *Green Chem.* **17**, 1492–1499 (2015).
52. Stein, J. S., Holmgren, W. F., Forbess, J. & Hansen, C. W. PVLIB: open source photovoltaic performance modeling functions for Matlab and Python. In *2016 IEEE 43rd Photovoltaic Specialists Conference (PVSC)* 3425–3430 (IEEE, 2016).

Acknowledgements

This work is supported by the Sustainable Food, Energy, and Water Systems programme, funded by National Science Foundation Research Traineeship Award 1735282.

Author contributions

C.K.M. and R.A. developed the initial land-area estimation model, conceptualized the aglectric PV systems and estimated the power output of these systems. Y.L. refined and finalized the land-area estimation model. Y.L. and R.A. analysed the synergy of PV and wind aglectric farming, drafted the associated results and compiled the author contributions. A.P. developed the shadow depth model and simulation with consultation from P.B. and E.K.G. R.G.E. provided the schematics of land-area estimation and innovative PV systems. R.A. directed the overall research. All authors assisted in drafting and editing the final manuscript.

Competing interests

The authors declare no competing interests.

Additional information

Supplementary information is available for this paper at https://doi.org/10.1038/s41893-019-0388-x.

Correspondence and requests for materials should be addressed to R.A.

Reprints and permissions information is available at www.nature.com/reprints.

Publisher's note Springer Nature remains neutral with regard to jurisdictional claims in published maps and institutional affiliations.